Comparison of local methods to detect vorticity in RANS simulations of the flow in the wake of a marine propeller

Laurens-Jan Roos

April 10, 2013

Abstract

The comparison between different methods to identify the wake vorticity structure from a RANS calculation of the flow around a marine propeller. Three methods are considered, vorticity magnitude, Q-factor and total pressure variation.

Of these methods the total pressure variation method turned out to give the most reasonable results, whereas Q-factor method showed some problems with the accuracy. The total vorticity method showed good results and was stable for the whole range of advance ratios.

1 Introduction

For turbo-machinery the correct simulation of the flow is essential for performance analysis. Especially the wake structure is important, as the induced velocity on the propeller blades is much larger than the induced velocity on an aircraft wing. [1]

These wake structures are captured by Navier-Stokes as they fully describe the flow. As a full Navier-Stokes simulation is very computational expensive, the Reynolds averaged Navier-Stokes (RANS) equations are used instead to calculate the flow field.

While these RANS simulations are able to capture all the phenomena in the solution, it still takes a considerable calculation time. Therefore, it is preferred to use a panel flow in combination vortex sheets to model the wake structure. For the panel flow simulation the vortex sheets have to be added as a boundary condition, but the problem is that the position can not be know on forehand.

In this paper, we will look into a few methods to extract the tip vortex positions from a RANS solution. Fits of these positions at different flow conditions could then be used in panel flow simulations.

2 Theory

Due to the pressure difference between the pressure side and the suction side of the blade, a tip vortex will appear at the edge of the blade. Also at the the trailing edge a vortex appears, which together form a vortex sheet. Due to the rotational motion of the blades, the vortex sheet modeling the wake looks like a helix as shown in figure 1. The vortex sheet of all the blades forms the wake, which influences the inflow angle at the blade which will in turn affect the produced thrust and torque.

The radius of the helix decreases after the propeller since the velocity after the propeller increases. Far downstream ratio between the

radii should be inverse proportional to the ratio of the velocities.

The pitch is influenced by the angle of attack. If we assume a frontal flow, the flow conditions are given by the flow number J, which is defined as $J = \frac{V_{ref}}{nD}$, with V_{ref} taken at 70% of the blade radius; n the rotational speed and D the diameter. At the design flow number, the pitch length of the wake should be the same as the advance ratio of the propeller. A lower flow number means that the flow has a higher angle of attack, thus the pitch will be smaller.

However the pitch is not constant over the radius. Near the root (of the blade) the pitch increases faster, this is because influence of the vortex increases with radius. This means that the tip vortex "forces" the vortex near the root down. This can be seen in figure 1. In practice however this effect is small.

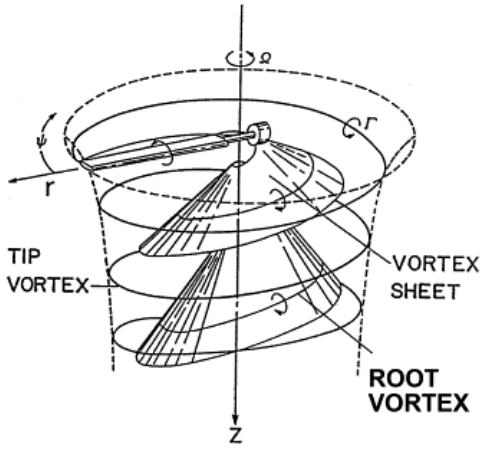

Figure 1: Schematic picture of the wake structure, in this case of an helicopter rotor

The strength is determined by the amount of circulation around the blade, this circulation is determined by the amount of lift (in this case thrust) generated.

As the edge of the vortex sheet is formed by the tip vortex, we only have to find that to find the shape of the sheet. According to [2], the following characteristics are commonly used for a vortex core:

- Total pressure minimum
- High vorticity
- High ratio between rotation and shear

Each of the detection methods described in section 4.1 are based on one of these characteristics.

3 Description of problem

The propeller in the provided datasets is an uncased propeller with four forward-angle blades with a advance ratio of 1.06 at a design flow number of 0.71. The flow around it is calculated by *Refresco*, a finite volume RANS solver from Marin institute in Wageningen.

The flow has a uniform velocity inflow and has no pre-swirl. In the datasets provided, only the inlet velocity V_∞ is changed, the rotational speed Ω and diameter D remain the same. The pressure at all boundaries is set at zero.

A Cartesian coordinate system (figure **??**) is used to describe the flow, with the propeller in the Y-Z plane and the flow coming from the negative X-axis.

$$\frac{r}{R} = \frac{\sqrt{y^2+z^2}}{R} \quad (1)$$

$$\theta = \arctan(z/y) \quad (2)$$

$$\phi = \arctan(\frac{x_2 - x_1}{\theta_2 r_2 - \theta_1 r_1}) \quad (3)$$

$$\frac{p}{D} = \pi \frac{r}{R} \tan(\phi) \quad (4)$$

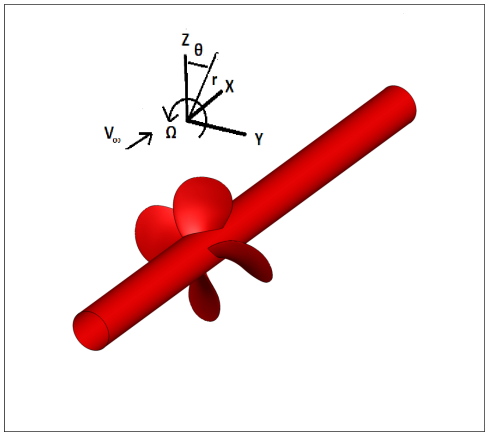

Figure 2: Schematic picture of the wake structure, in this case of an helicopter rotor

4 Methods

There are two main categories of methods to find the vortices: the local methods and the global methods. [3] The local methods only require the data of the cells at one slice in order to find the vortex, whereas global methods use also data in the third dimension. The latter would generate vortex filaments throughout the domain while the first finds discrete vortex positions in each slice. In this paper, we only concern ourself with the local methods.

The local methods here all follow the same basic steps: first some detection method is used to "light" up the tip vortex, then the peak is taken as the tip vortex. This process is done for different distances from the propeller. Some caution should be given as the global maximum value might be in the boundary layer region. Therefore it should be checked if the peak is in logical area. This whole process can be done manual or automatically. In this work it was done manually.

The radius, theta, pitch angle and pitch length are calculated by the equations 4 using these extracted positions.

4.1 Detection methods

4.1.1 Total vorticity

The vorticity magnitude is taken as the second vector norm of the vorticity vectors in ω_x, ω_y and ω_z.

$$|\omega| = \sqrt{\omega_x^2 + \omega_y^2 + \omega_z^2} \tag{5}$$

In [2], it is argued that the vorticity magnitude does not detect all kinds of vortices, especially when they are near solid walls. This makes it difficult for detecting boundary layers.

If there are multiple vortices close to each other, they might get cancelled out.

4.1.2 Q-factor

The Q-factor gives the balance between rotation and stretching of a fluid element. The dimension full form is given by:

$$Q = \tfrac{1}{2}(\|\Omega\|^2 - \|S\|^2) \tag{6}$$

The two components written out in the Cartesian velocity gradients are:

$$\|\Omega\| = tr(\Omega\Omega^T) = \tfrac{1}{2}(\omega_x^2 + \omega_y^2 + \omega_z^2) \tag{7}$$

$$\|S\| = tr(SS^T) = u_x^2 + v_y^2 + w_z^2 \tag{8}$$

$$+ \tfrac{1}{2}(u_y^2 + v_x^2 + 2u_y v_x) \tag{9}$$

$$+ \tfrac{1}{2}(u_z^2 + w_x^2 + 2u_z w_x) \tag{10}$$

$$+ \tfrac{1}{2}(w_y^2 + v_z^2 + 2v_z w_y) \tag{11}$$

The $\|\Omega\|$ corresponds to the amount of vorticity, whereas $\|S\|$ corresponds to the amount of stretching. At vortex centres, the Q-factor should be very large, since the vorticity term is there much larger than the stretching term. At the wall the Q-factor should be zero.

The non-dimensional form of the Q-factor is:

$$\bar{Q} = \tfrac{1}{2}\left(\frac{\|\Omega\|^2}{\|S\|^2} - 1\right) \tag{12}$$

To avoid division through zero, a very small value is added to the symmetric part.

4.1.3 Total pressure variation

This method is based on the property that vortex cores have a lower total pressure in the centre than in their surroundings.

The total pressure variation for a flow with an upstream speed along the axis and rotating blade at speed Ω.

$$\Delta p_t = p + \tfrac{1}{2}\rho(v_x^2 + \tag{13}$$
$$(v_y + r\Omega\sin\theta)^2 + (v_z - r\Omega\cos\theta)^2) \tag{14}$$
$$-p_{\text{inf}} - \tfrac{1}{2}\rho U_{\text{inf}}^2 + r\Omega \tag{15}$$

In order to account for the rotation of the blades, the rotational speed is subtracted. The total pressure variation is made dimensionless by:

$$C_{\Delta p_t} = \frac{\Delta p_t}{\frac{1}{2}(\rho U_{\text{inf}}^2 + r\Omega)} \tag{16}$$

Only in the boundary layer and the tip vortices the coefficient should be negative, everywhere else in a region of constant total pressure it should be equal to zero as the two terms cancel each other out.

4.2 Fitting model

The found positions are fitted around a helix along the x-axis with a decreasing radius and increasing pitch. Instead of the pitch, the angle theta could also be used, but this is not conventional. The equations for the helix are:

$$y(x/R) = R\frac{r}{R}(x/R)\sin\theta(x/R) \tag{17}$$
$$z(x/R) = R\frac{r}{R}(x/R)\cos\theta(x/R) \tag{18}$$

where $\frac{r}{R}(x/R)$ and $\theta(x/R)$ represent the found fits.

According to [1], the radius decreases till it reaches a stable condition. He used different fit for the unsteady and steady part.

The steady part is modeled by

$$\frac{r}{R} = A - \frac{B}{J} \tag{19}$$

with A and B constants to be determined from the results.

The unsteady part is somewhat trickery, as there is no consensus how the radius decreases. In [1] a fit without background theory is being used for the unsteady part. In this work a power function is used to model the radius.

$$\frac{r}{R}(x/R) = A \cdot (x/R)^B + C \tag{20}$$

with A, B and C constants to be determined from the results.

The theta is modeled by a second order polynomial as the angular velocity is expected to slow down as we get farther from the propeller.

$$\theta(x/R) = A \cdot (x/R)^2 + B \cdot (x/R) + C \tag{21}$$

with A, B and C constants to be determined from the results.

5 Results

In table 1 we can see a comparison of isosurfaces. Both the total vorticity and total pressure variation show clearly the helical spiral of the tip vortex, as well as the boundary layer around the blades and the shaft. The isosurface of the Q-factor however only shows the helical wake. While this is expected, the cross area of the wake seems to change more abruptly than with the other methods.

All show that the wake structure is contracting due to the energy added to the fluid by the propeller. All these wakes slowly converge into one large cylindrical wake.

In figures 2, 3 and 4 the development of the tip vortex under different methods can be seen.

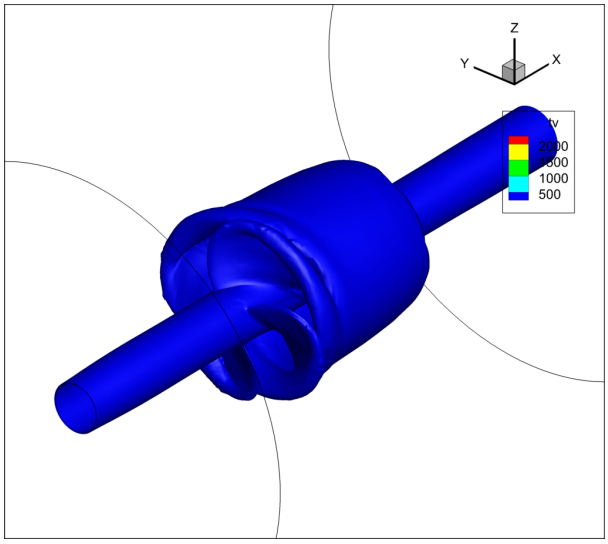

Total vorticity with threshold at 1.0

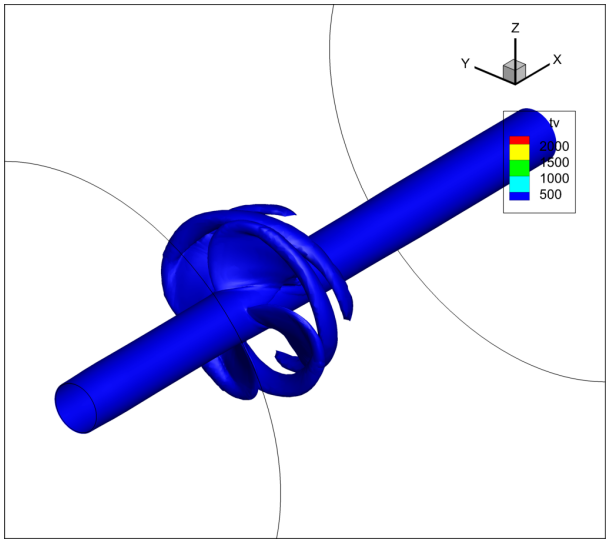

Total vorticity with threshold at 2.0

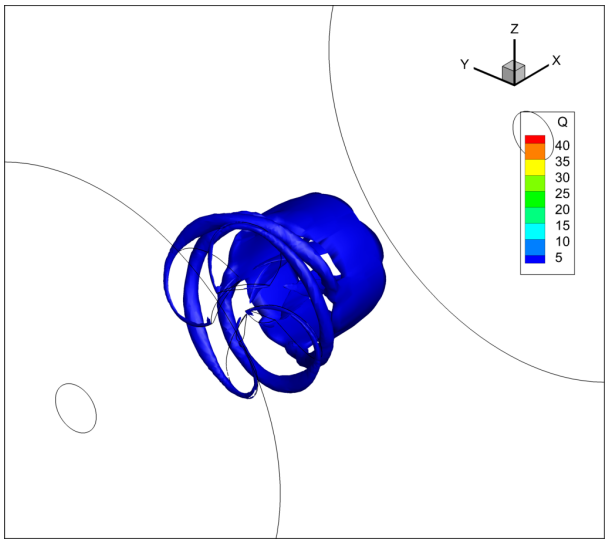

Q-factor with threshold at 0.5

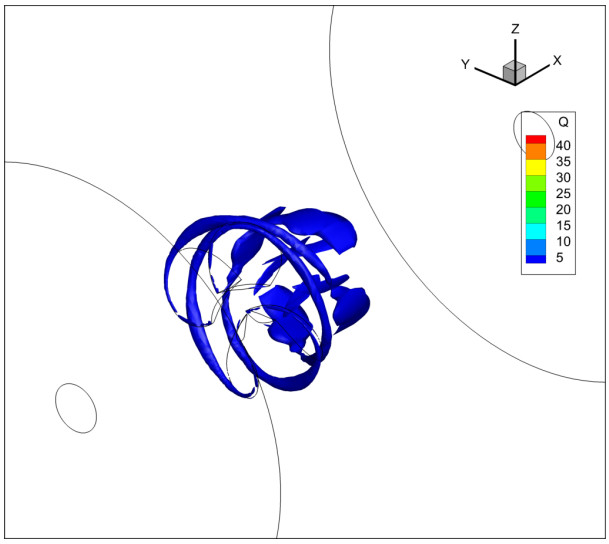

Q-factor with threshold at 1.0

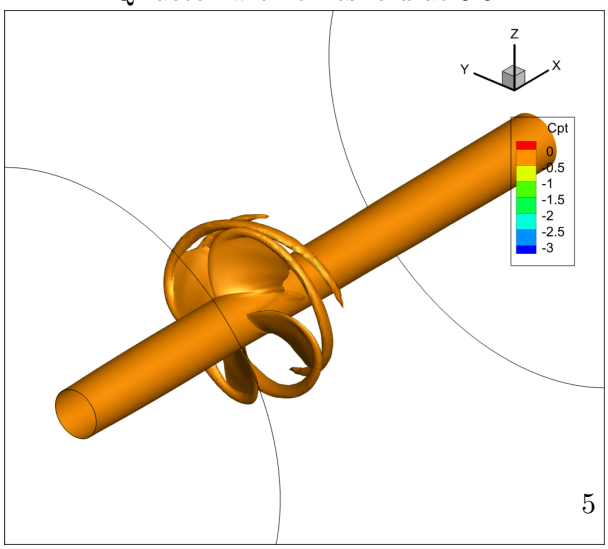

Cpt with threshold at -0.3

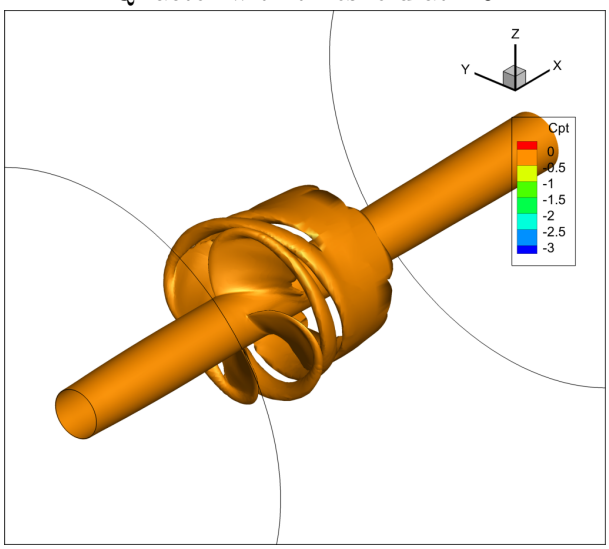

Cpt with threshold at -0.2

Table 1: Comparison of isosurfaces at J=0.20

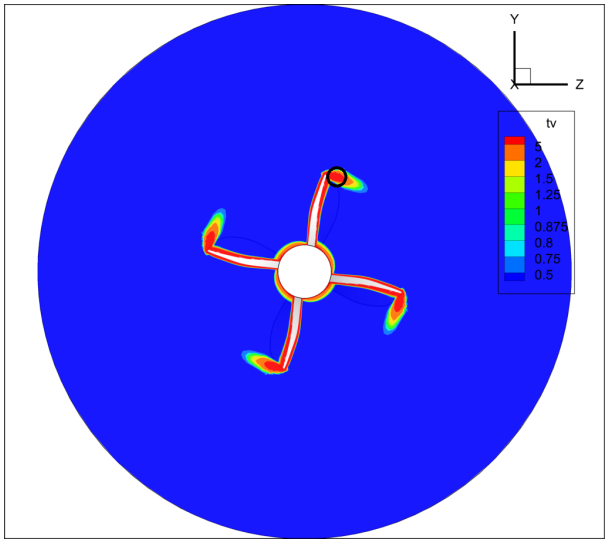

TV, $x/R = 0.00$

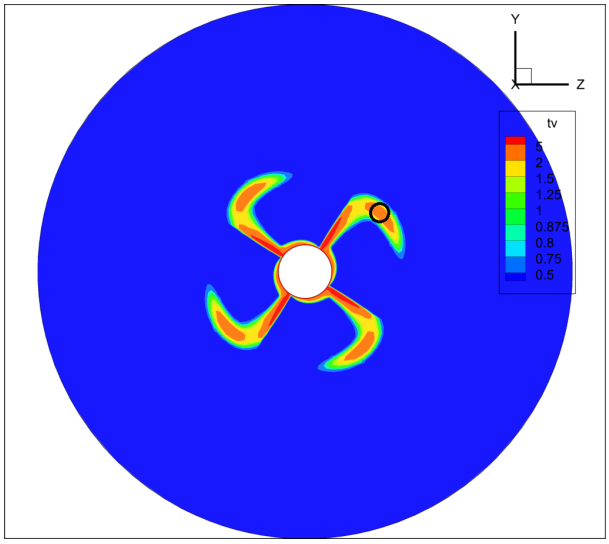

TV, $x/R = 0.18$

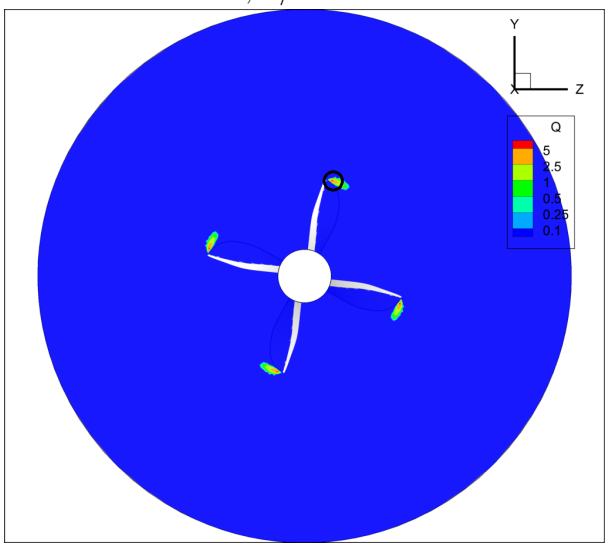

Q, $x/R = 0.00$

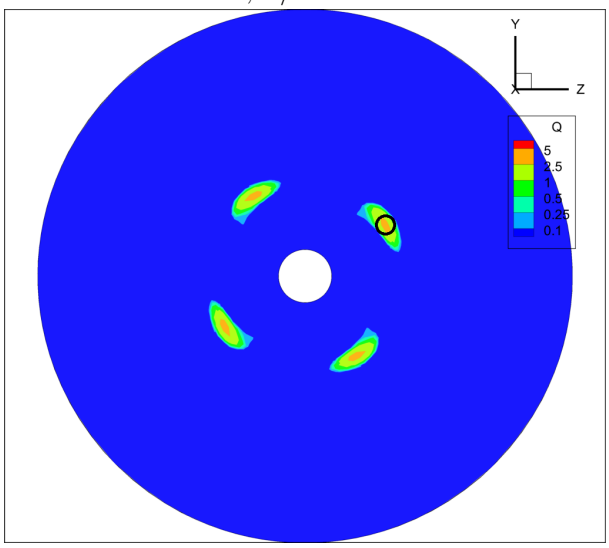

Q, $x/R = 0.18$

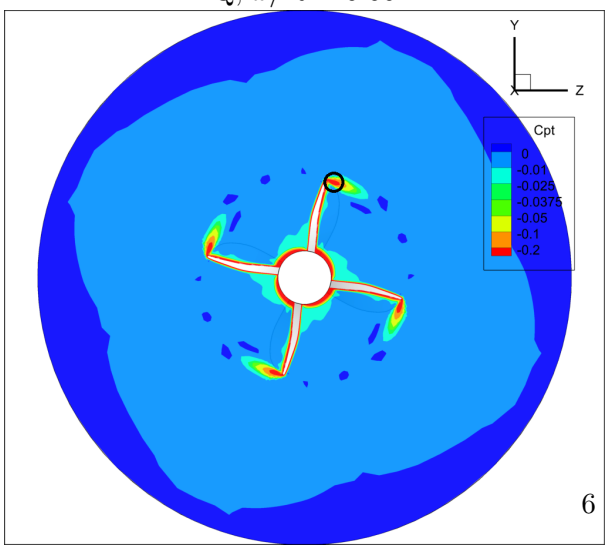

Cpt, $x/R = 0.00$

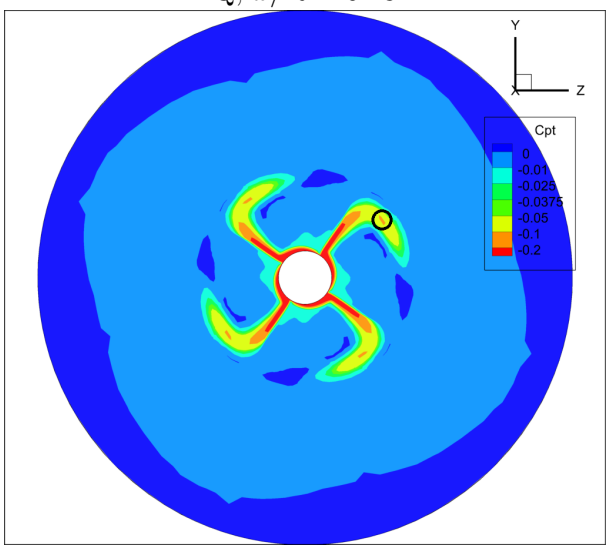

Cpt, $x/R = 0.18$

Table 2: Slices for different methods at different distances behind the propeller. J=0.71 The black circle indicates position of one tip vortex.

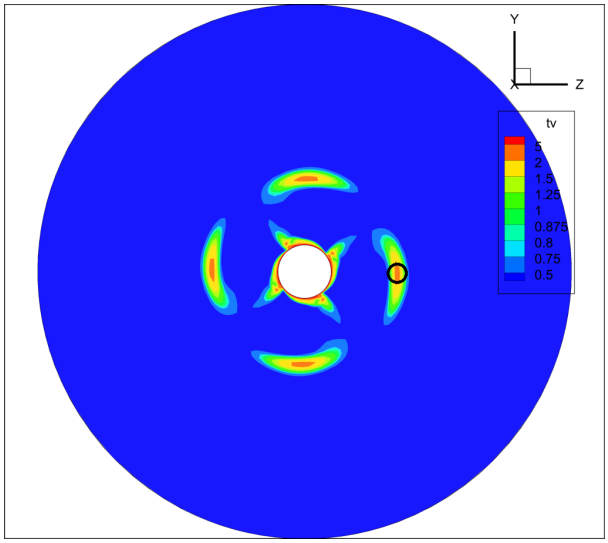

TV, $x/R = 0.35$

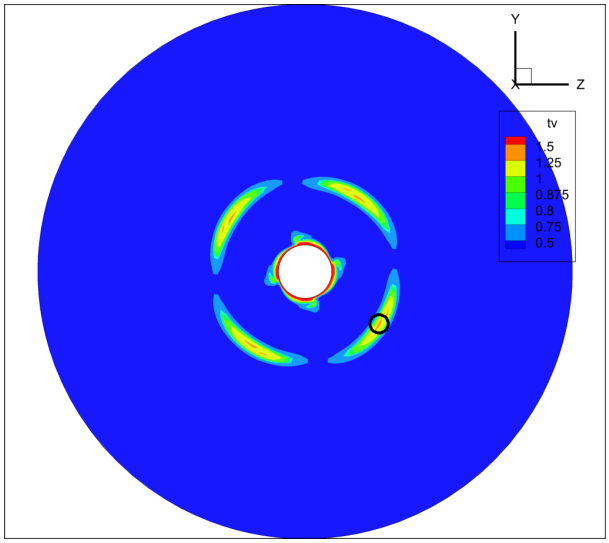

TV, $x/R = 0.53$

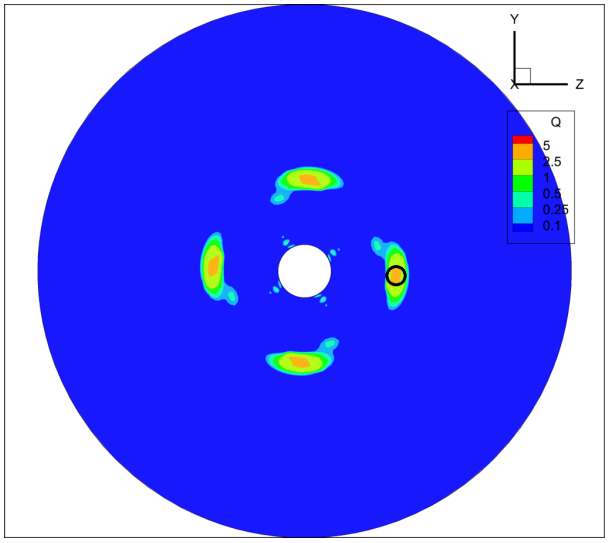

Q, $x/R = 0.35$

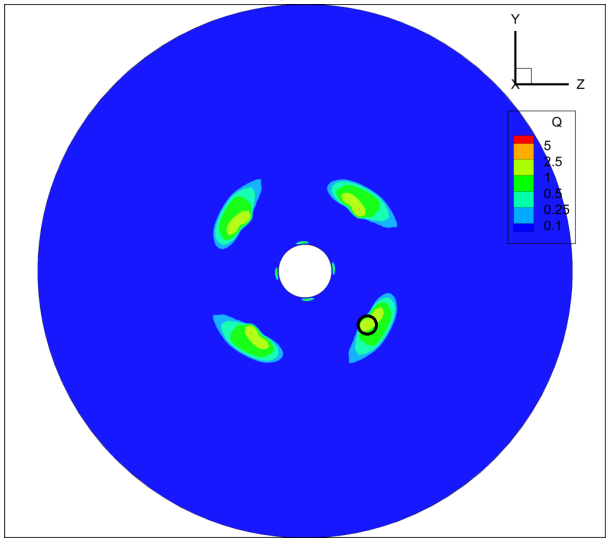

Q, $x/R = 0.53$

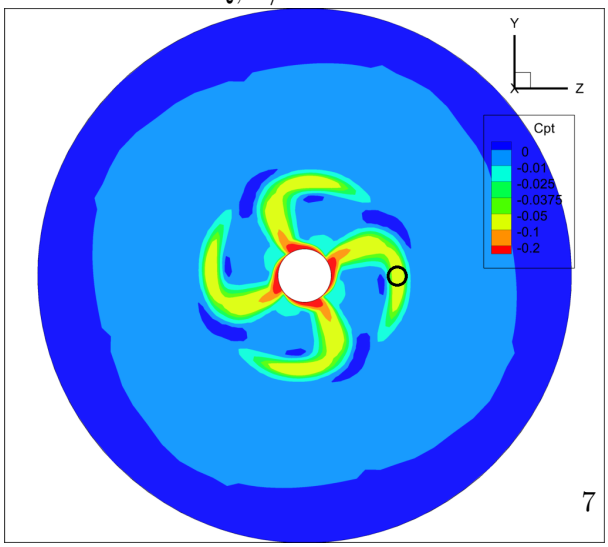

Cpt, $x/R = 0.35$

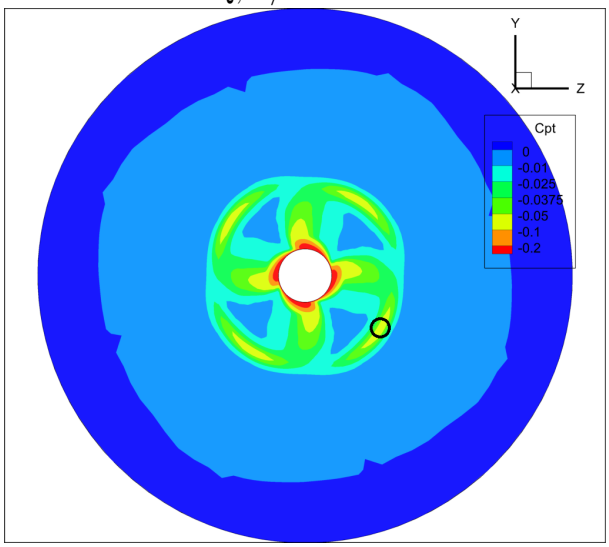

Cpt, $x/R = 0.53$

Table 3: Slices for different methods at different distances behind the propeller. J=0.71 The black circle indicates position of one tip vortex.

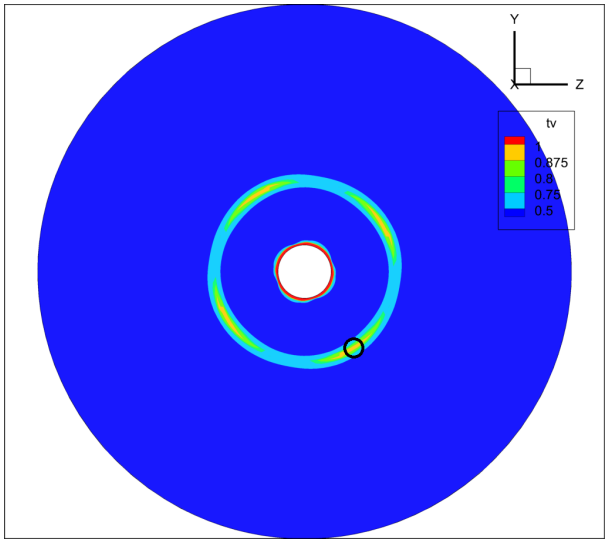

TV, $x/R = 0.70$

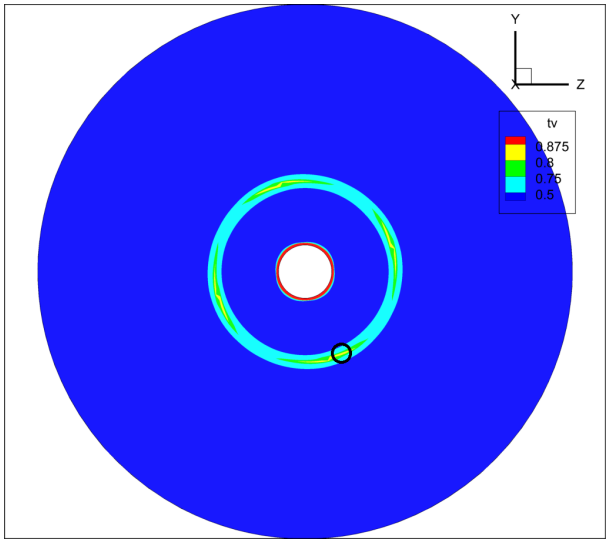

TV, $x/R = 0.88$

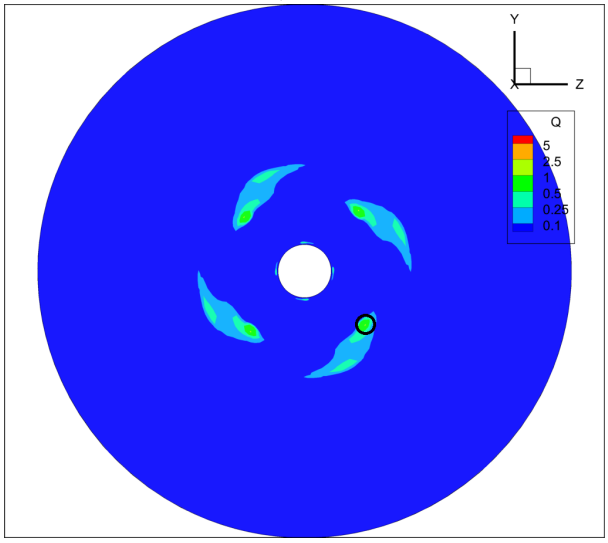

Q, $x/R = 0.70$

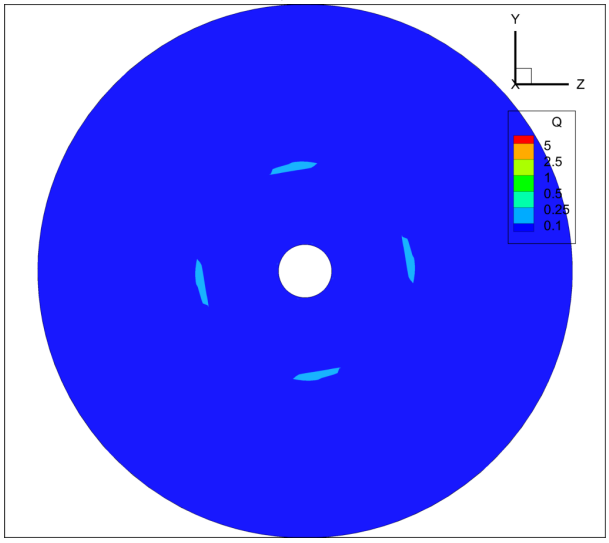

Q, $x/R = 0.88$

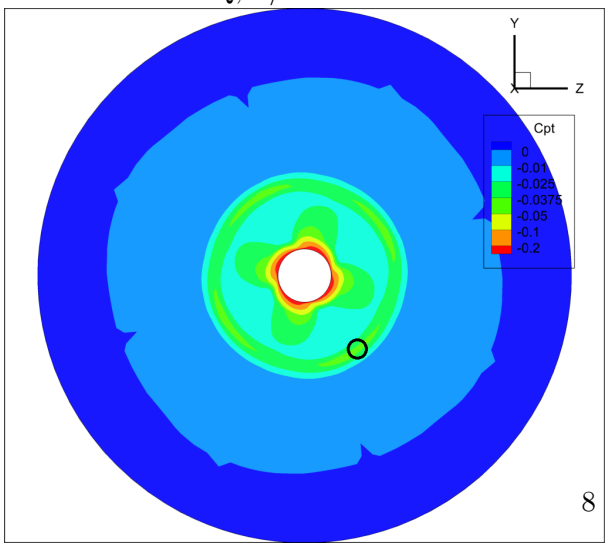

Cpt, $x/R = 0.70$

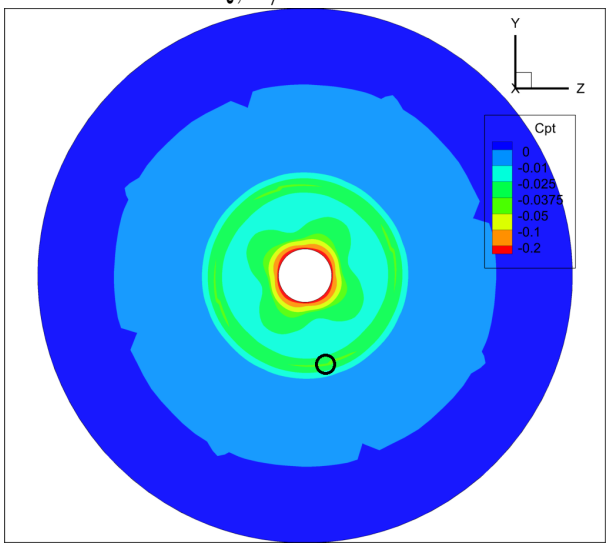

Cpt, $x/R = 0.88$

Table 4: Slices for different methods at different distances behind the propeller. J=0.71 The black circle indicates position of one tip vortex.

Whereas the Q-factor method does not show the wake behind the propeller blades and the boundary layer as expected [2], the other two methods clearly show the wake behind the propeller blades. Also the other two methods show the boundary layer more prominently than a Q-factor method.

It can be seen that in the tip vortex, two areas seem to appear. In the first one the top is in the front one, but in the second one the peak value is in the area behind. This might cause the sudden drop in the radius.

As seen in the isosurface plots and at the end of series of slices, the tip vortices merge after some distance travelled into one ring. This makes it very difficult to estimate the theta of the tip vortex farther aft this point.

The peak values tend to rapidly decrease for the total vorticity and total pressure method, but the peak value of Q-factor tends to decrease much slower. For low threshold values for Q, there is also a large ring visible at the end of the domain.

6 Extracted data

The calculated radius shows that the tip vortex radius decreases with the distance from the propeller. The total vorticity method and the total pressure method show similiar results, but the radius calculated by the Q-factor method changes significantly after $x/R = 0.6$. For lower advance ratios, it settles at about 80% of the other methods. For higher J-values the effect is inversed as the radius calculated by the Q-factor method *increases* with the distance from the propeller.

The theta increases with x, but the rate at which it increase slowly decreases. Here all methods seems to agree upon. The pitch angle seems to be almost constant for the whole range. Only at the end there is a jump in the pitch angle.

The pitch distance is the same for all methods as can be seen in figure 3. The problem of the pitch formula is that it is sensitive to small oscillations in the angle theta and radius. We can see that the value is around the advance ratio of the propeller (1.06).

6.1 Values for different flow conditions

The correlation between radius and the flow conditions seems to increase linearly. The point where the limiting value is reached, is nearer to the propeller for lower flow conditions. The steady radii to converge for higher advance ratios.

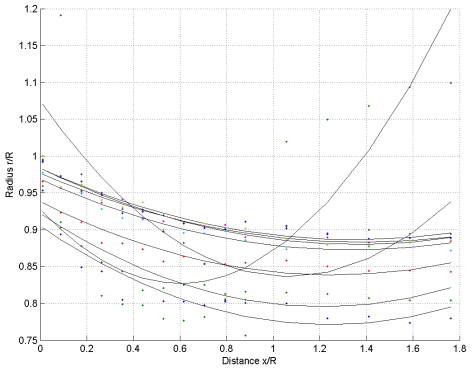

Figure 4: Comparison of fits of radius for different flow conditions

The theta fit increases with the increasing flow conditions. The rate of decay of the slope of the fit is approximate the same for all flow conditions.

The calculated pitch angle fit increases with increasing J-values. The pitch fit increases with increasing J-values. This makes sense as the

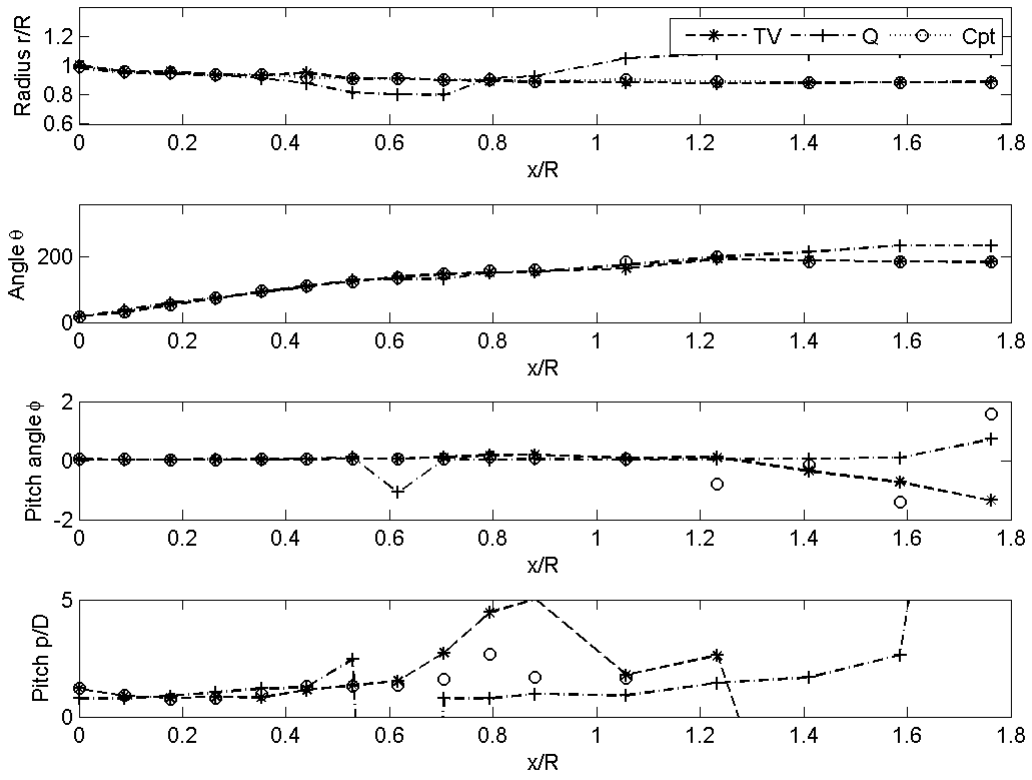

Figure 3: Comparison of different methods for J=0.71

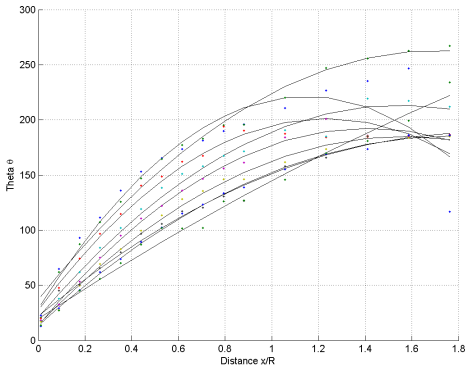

Figure 5: Comparison of fits of theta for different flow conditions

angle of attack becomes higher with higher J-values, thus the pitch tend to be stretched in the longitudinal direction.

The found fits for radius and pitch follow a similar trend as in [1]. While the values are of the same order of magnitude, it should be noted that in that paper a five bladed propeller is used. Moreover, the values are experimentally acquired in that paper.

7 Discussion

As indicated in the results, the difference between values becomes very small as shown in figure, it is very difficult to extract the positions far downstream. This makes it difficult to assess if it is still in the transition zone.

As said before, the quality of the Q-factor seems to be dependent upon the J-value. However, the other methods suffer also from the problem that for higher J-values, the differences become smaller. This makes it harder to detect the peaks.

According to [4] the RANSE simulation introduces more viscosity by not modeling the turbulence and therefore the tip vortex decays faster. This would also explain the decreasing peak values at the slices. Therefore it would be interesting to see how the results change if another type of simulation is used.

Another problem is that there is no higher resolution grid available, thus a Richardson extrapolation to estimate the order of error is impossible. Even if there was, then it would be difficult to distinguish between errors in the solver and errors in the detection method.

For further research into this subject, more refined grids would be necessary.

As we can see in the results of the fit for the radius, that it is not so good. This could be explained by the manual selection of points, but this would not explain the large deviations in radius, but not theta. Unfortunately these deviations cause larger deviations in the pitch angle and pitch.

As indicated in the results, the Q-method sometimes gave *two* peaks instead of one. This would suggest that there are two vortices. The other two methods do not show this. It is the question if this is just a numerical artifact or really happening in the flow.

This phenomenon might be explained as a vortex with an shear flow, which creates two peaks instead of one.[2] Also these peaks are perpendicular to the position of the real peak, which could explain this effect.

Another explanation is that since the vortex core is moving in time due to the rotational speed of the propeller, the tip tends to be smeared out over a small area. This might be explained the behaviour of drop of the radius with the Q-factor method. The Q-factor method generated a peak at the tail of the vortex as the core instead of the core itself.

On advantage Q-factor has over other methods is that is does not show the boundary layer around the horizontal shaft nor the wake after

the propeller blades. This would be advantageous in automatic vortex detection.

8 Conclusions

As seen in the results, the total vorticity method and coefficient of total pressure show similar results. The Q-factor, while useful to find the region where the tip vortex is located, gives worse results for the radius. Also the "stability" is highly dependent on the advance ratio. Therefore is the Q-factor not advised for tip vortex extraction.

Since the results from total pressure variation and total vorticity are quite similar, the question arises which method would get preference. As the total pressure variation takes the rotation into account, it is preferred. The total pressure variation however has as drawback that at higher values of J, the tip vortex becomes less clear. Therefore the total vorticity has preference as it works for the whole range of advance ratios.

References

[1] T. Hoshino. Hydrodynamic analysis of propellers in steady flow using a surface panel method. *Journal of the Society of Naval Architects of Japan*, 165(6):55–70, 1989.

[2] Jinhee Jeong and Fazle Hussain. On the identification of a vortex. *Journal of Fluid Mechanics*, 285, 1995.

[3] Ming Jiang, Raghu Machiraju, and David Thompson. Detection and visualization of vortices. In *The Visualization Handbook*, pages 295–309. Academic Press, 2005.

[4] R. Muscari, A. Di Mascio, and prof.dr. R. Verzicco. Modeling of vortex dynamics in the wake of a marine propeller. *Computers and fluids*, 73:65 – 79, 2013.

Appendix

Results for all the flow conditions

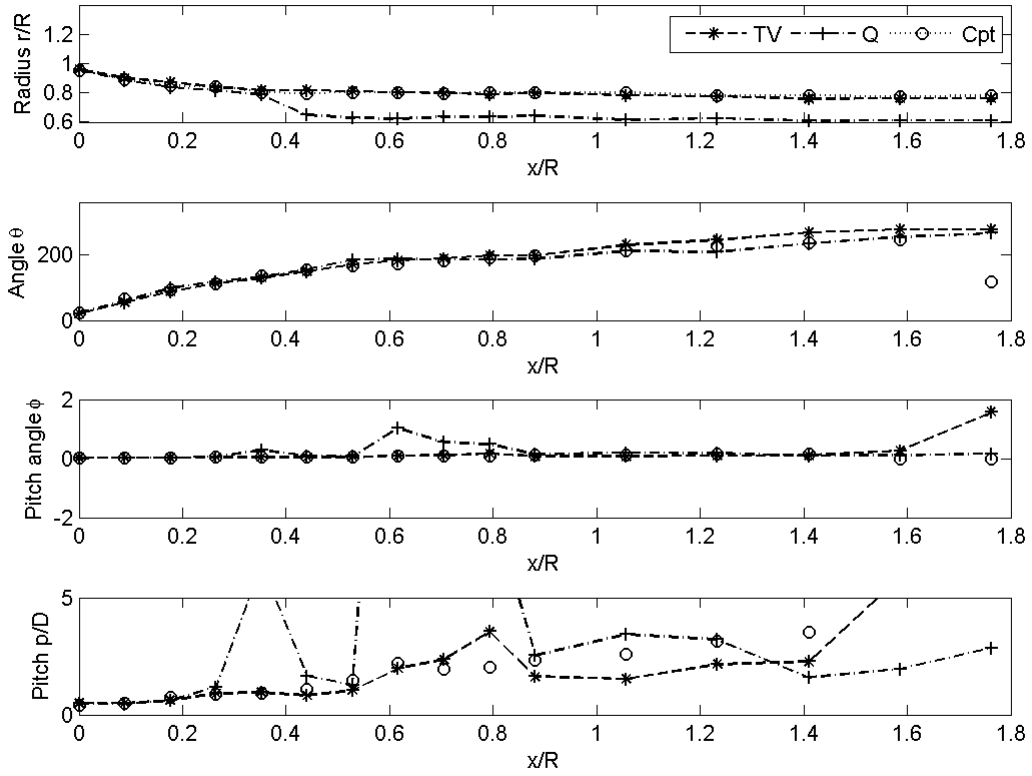

Figure 6: Comparison of different methods for J=0.10

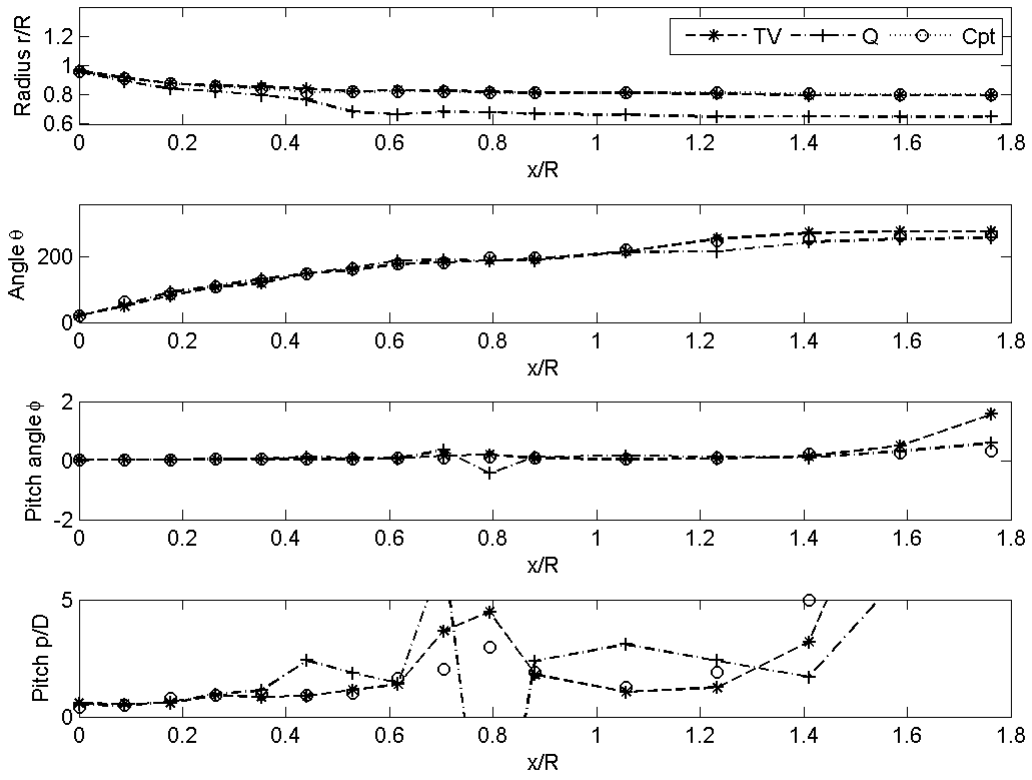

Figure 7: Comparison of different methods for J=0.20

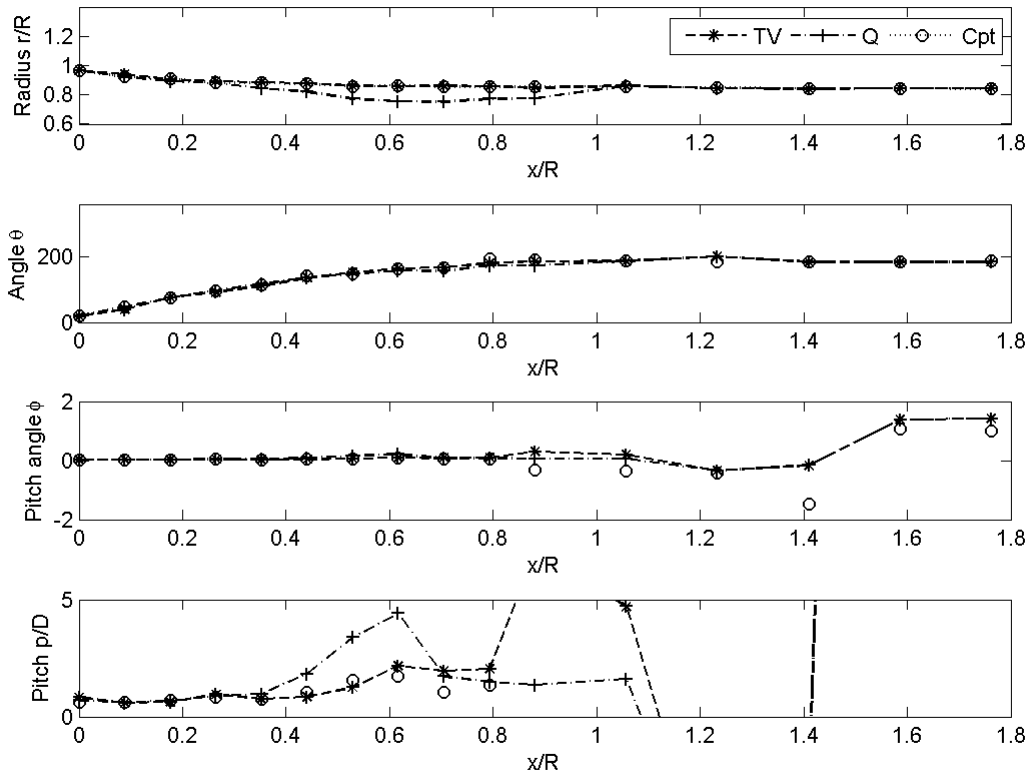

Figure 8: Comparison of different methods for J=0.40

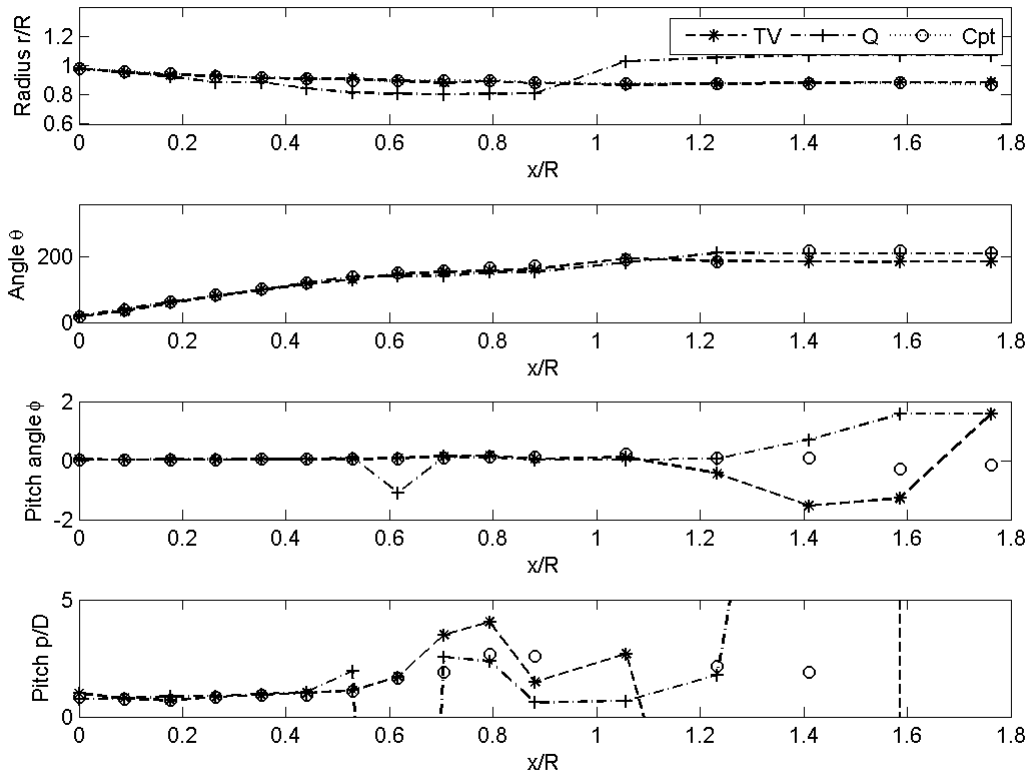

Figure 9: Comparison of different methods for J=0.60

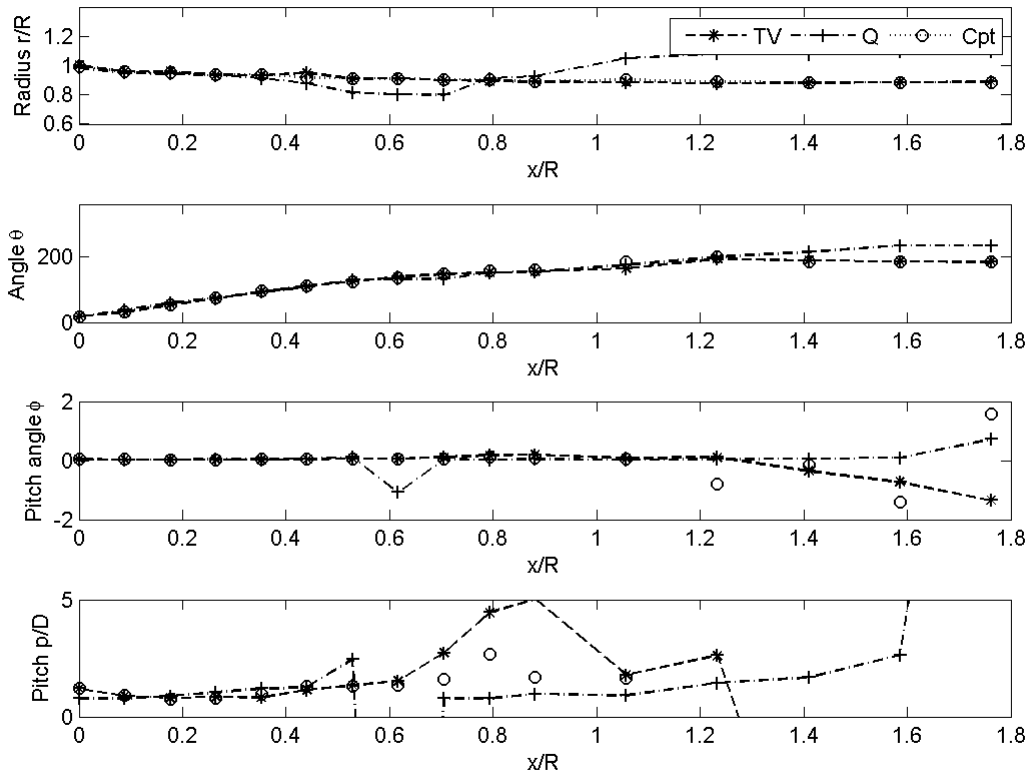

Figure 10: Comparison of different methods for J=0.71

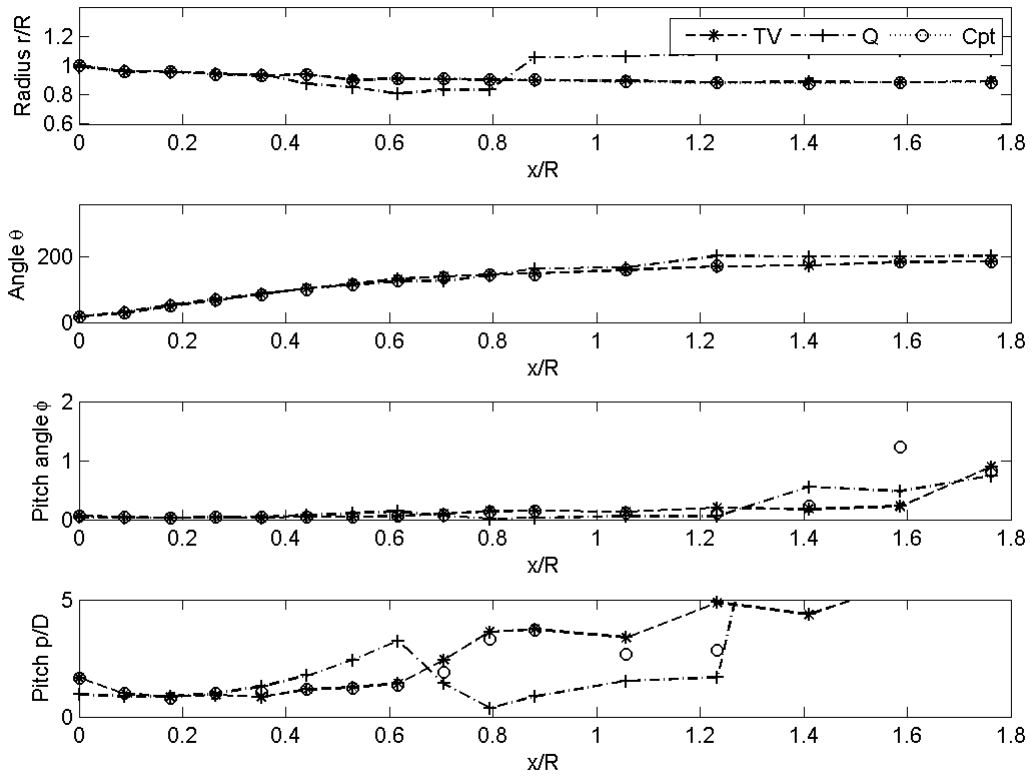

Figure 11: Comparison of different methods for J=0.80

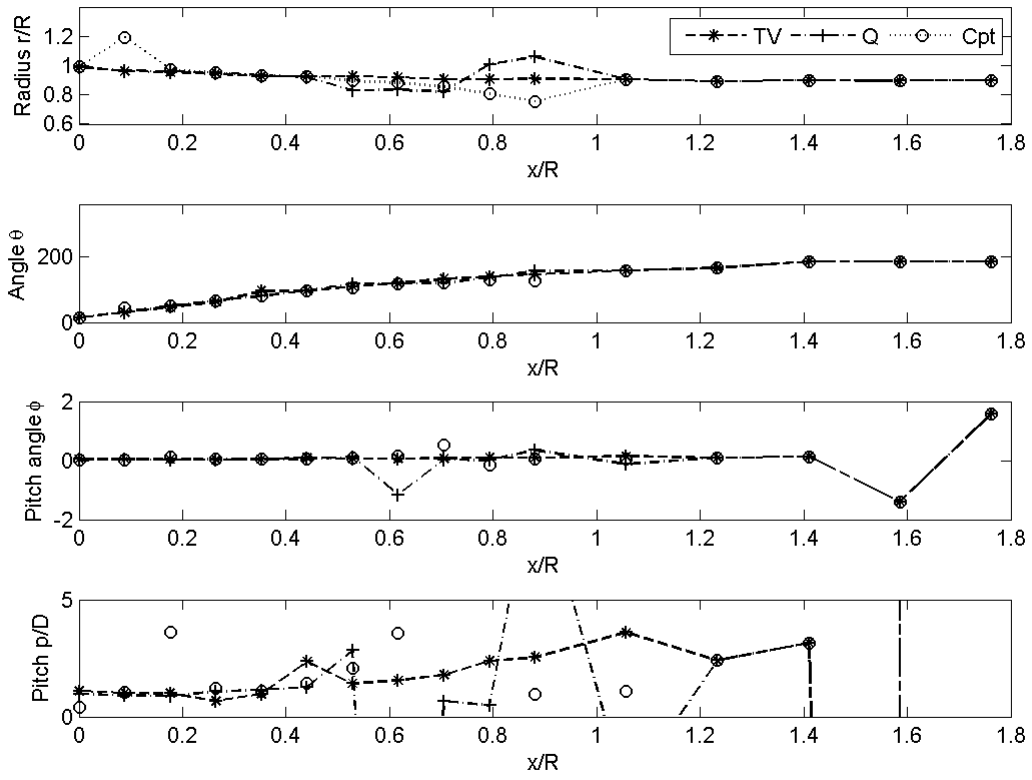

Figure 12: Comparison of different methods for J=0.90